

Marechal, L.; Shaohui Foong; Shuoyu Ding; Madhavan, D.; Wood, K.L.; Gupta, R.; Patil, V.; Walsh, C.J., "Optimal spatial design of non-invasive magnetic field-based localization systems," *Robotics and Automation (ICRA), 2014 IEEE International Conference on*, pp.3510-3516, May 31 2014-June 7 2014

<http://ieeexplore.ieee.org/stamp/stamp.jsp?tp=&arnumber=6907365&isnumber=6906581>

© 2014 IEEE. Personal use of this material is permitted. Permission from IEEE must be obtained for all other uses, in any current or future media, including reprinting/republishing this material for advertising or promotional purposes, creating new collective works, for resale or redistribution to servers or lists, or reuse of any copyrighted component of this work in other works.

Optimal Spatial Design of Non-Invasive Magnetic Field-Based Localization Systems*

Luc Maréchal, Shaohui Foong, *Member, IEEE*, Shuoyu Ding, Dushyanth Madhavan
Kristin L. Wood, Rajiv Gupta, Vaibhav Patil, and Conor J. Walsh, *Member, IEEE*

Abstract—Magnetic localization systems based on passive permanent magnets (PM) are of great interest due to their ability to provide non-contact sensing and without any power requirement for the PM. Medical procedures such as ventriculostomy can benefit greatly from real-time feedback of the inserted catheter tip. While the effects of the number of sensors on the localization accuracy in such systems has been reported, the spatial design of the sensor layout has been largely overlooked. Here in this paper, a framework for determining an optimal sensor assembly for enhanced localization performance is presented and investigated through numerical simulations and direct experiments. Two approaches are presented: one based on structured grid configuration and the other derived using Genetic Algorithms. Simulation results verified by experiments strongly suggest that the layout of the sensors not only has an effect on the localization accuracy, but also has an effect far more pronounced than improvements brought by increasing the number of sensors.

I. INTRODUCTION

Magnetic field-based localization systems are used widely in robotics and automation for online and contact-free tracking of all kinds of devices and objects. The human body is not affected by static fields, which are generally regarded as safe. Recently a plethora of new developments in biomedical and surgical applications have taken advantage of this to make use of magnetic field based sensing technology to localize instruments and track them non-invasively in real time while deep inside the body. Such tool will also pave the way for clinical procedures to be performed with high precision with robotic assistance or even by a fully automated system. Much research has been pursued to enhance the performance of magnetic localization through improved algorithms and field models [1], [2]. But a key element, the design of the magnetic sensor assembly, and in particular, the spatial design of the sensor network, has been largely overlooked and neglected. Hence this paper is focused on the spatial optimization of a magnetic localization system for enhanced performance.

The insertion of flexible catheters into the body is an excellent example of a procedure that can benefit from magnetic

localization technology. Ventriculostomy is a neurosurgical procedure that involves inserting a catheter through a burr hole on the skull to access the ventricles for drainage. Although this procedure is conducted by skilled and experienced practitioners, placement accuracy is low because the insertion is performed blindly and the clinician has no visual feedback of the location of the catheter tip. It is not uncommon to require multiple passes to reach the target, with each unsuccessful and misplaced pass increasing the likelihood of morbidity and hemorrhagic complications [3]. By embedding a small permanent magnet (PM) at the distal tip of the cannula or the stylet guiding the catheter, external magnetic sensors can be employed to determine the position of the magnet inside the head.

Several such magnetic localization systems utilizing passive magnets have been investigated in the last decade [4]–[7]. Almost all of these systems are based on a 2D-array of multi-axis sensors uniformly arranged on a square grid pattern. While there has been considerable analysis concerning the number of sensors on localization performance [8], [9], questions remain regarding the spatial design component of the sensing system. For example, even if a square grid arrangement could be justified, there is no scheme to determine the optimal grid spacing. It is possible that the lack of knowledge in this area can be attributed to the fact that these sensing systems were not designed for any specific application.

Ventriculostomy is a highly repetitive procedure in which the trajectory does not deviate significantly from one adult to another. For this kind of intervention, it is possible to design a sensing system based on a reference trajectory. The work presented here is aimed at developing a framework in which an optimized arrangement of sensors can be determined when the repetitive localization trajectory is known *a priori*. Ventriculostomy catheter insertion is used as an example in this paper.

A key issue in searching for an optimal arrangement of sensors, especially when the number of sensors is large, is that traditional calculus-based and enumerative search algorithms are inefficient and biased to local stationary points. Thus genetic algorithms (GAs) which are often used to solve non-deterministic optimization problems due to their ability to search a wide range of the solution space rapidly [10], are incorporated into our approach.

The remainder of the paper presents:

- 1) An approach that seeks to determine an optimal configuration of field sensors while taking into consideration

*Research Supported by A*STAR-CIMIT Joint Grant 122440002 and SUTD-ZJU Research Collaboration Grant ZJURP1200102.

L. Maréchal, S. Foong †, S. Ding, D. Madhavan and K. L. Wood are with the Engineering Product Development Pillar at the Singapore University of Technology and Design (SUTD), Singapore.

R. Gupta and V. Patil are with the Center for Integration of Medicine & Innovative Technology (CIMIT), Boston, MA.

C. J. Walsh is with the Faculty of the School of Engineering and Applied Sciences, Harvard University, Cambridge, MA.

† Corresponding author email: shao@sutd.edu.sg

a reference trajectory.

- 2) Two contrasting spatial design schemes, one based on optimizing a structured rectangular grid pattern and another pattern achieved using GAs.
- 3) Numerical and experimental evaluation of a rectangular-based and GA-derived sensing system.

II. SPATIAL DESIGN OF MAGNETIC LOCALIZATION SYSTEM

The majority of magnetic localization systems that feature an untethered PM tracked by a spatial set of sensors are designed with the magnetic sensors distributed evenly and regularly in a grid within a 2D plane. Here an alternate approach is described, which takes into consideration the target trajectory, to determine an optimal configuration of sensors constrained in a rectangular grid arrangement and an unconstrained option using GAs. While the localization of a catheter inside brain is used as a scenario to illustrate this method can be applied to other applications such as tracking of robotic endoscopes and steerable needles.

A. Representative Trajectory

The mean distance traveled by the catheter tip from the burr entry hole to the ventricles during interventional procedures has been estimated to be 55-60 mm [11] while the distance, as measured by 78 fellows and residents, in a virtual reality workstation was an average of 63.63 mm [12]. These studies reveal that the distance traveled has relatively low variance and a representative trajectory can be used for the basis of design of a localization and tracking system.

Using a set of CT images of a fully inserted catheter in into the head of an anonymous patient and image processing software to perform segmentation to distinguish the foreign catheter, the path coordinates taken by the catheter, the catheter itself and the surrounding skull can be extracted. This segmentation was achieved using ImageJ [13]. Fig. 1(a) shows a sagittal CT image with the skull and catheter path highlighted in green and red respectively. With post-processing software, ITK-SNAP (www.itknap.org) [14], a 3D rendering of the skull and inserted catheter can be constructed as shown in Fig. 1(b), which allows the path to be characterized completely in the horizontal, coronal and sagittal anatomical 2D planes for development of the representative trajectory. The Euclidean distance between the burr hole and the tip of the fully inserted catheter was measured to be 60 mm.

B. Magnetic Field Modeling and Localization

The analytic dipole model is used widely to model permanent magnetic sources [4]–[6], [8], [15], [16]. Fig. 2 illustrates a single magnetic source in free space at $\mathbf{P}_m = (a, b, c)^T$ and its attached magnetic field detected by an arrangement of n sensors. The magnetic flux density, \mathbf{B} , is measured by the i^{th} sensor at $\mathbf{P}_{s,i} = (x_i, y_i, z_i)^T$,

$$\mathbf{B}(\mathbf{P}_{s,i}) = \frac{\mu_0 \cdot m_{DM}}{4\pi} \left[\frac{3\mathbf{P}_i(\mathbf{U} \cdot \mathbf{P}_i)}{|\mathbf{P}_i|^5} - \frac{\mathbf{U}}{|\mathbf{P}_i|^3} \right] \quad (1)$$

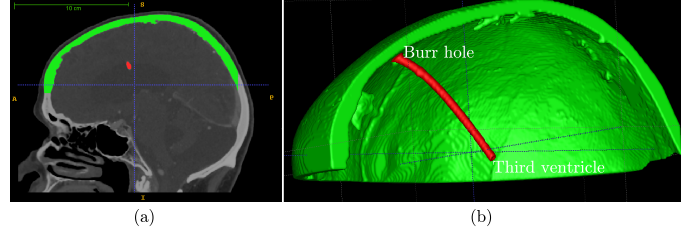


Fig. 1. (a) Sagittal CT image of a patient's head. (b) 3D rendering of part of the skull with an inserted catheter extending from the burr hole to the ventricles. The catheter (in red) is discriminated against the skull (in green).

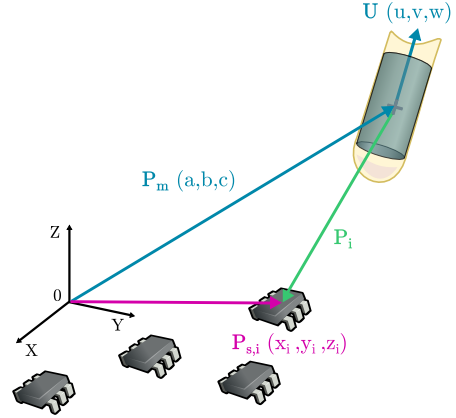


Fig. 2. Magnet Dipole Model. \mathbf{P}_m and $\mathbf{P}_{s,i}$ are the position coordinates of the magnet and i^{th} sensor, respectively with regard to the origin O . \mathbf{U} is the magnet's magnetization vector.

in which μ_0 is the magnetic permeability of free space, m_{DM} is the strength of the dipole moment of the magnet and $\mathbf{U} = (u, v, w)^T$ is the orientation of the magnetization vector of the magnet at \mathbf{P}_m . With this convention, the spatial vector denoting the direction and distance of each sensor from the magnet can be expressed as $\mathbf{P}_i = \mathbf{P}_{s,i} - \mathbf{P}_m$.

In localizing the position and orientation of the source, there are six unknowns in (1) which are a, b, c, u, v and w . However, for a large majority of magnetic sources, such as cylindrical magnets that possess axisymmetric geometry (magnetization axis coincides with the axis of symmetry), the magnetic flux density \mathbf{B} is also invariant about this axis. This constraint can be represented by

$$u^2 + v^2 + w^2 = 1 \quad (2)$$

which reduces the total number of unknowns to five. Hence, a minimum of five independent magnetic sensor measurements is required to determine the position and orientation of the unknown source. This can be achieved through a collection of single-axis sensors and/or multi-axis sensors.

If $\mathbf{B}_{measured,i}$ denotes the magnetic field measured at the location of the i^{th} sensor and $\mathbf{B}_{model,i}$ is the analytic model field in (1), the error function decomposed into the orthogonal components (x, y, z) is defined as:

$$E_{x,i} = \sum_{i=1}^N (B_{x, measured,i} - B_{x, model,i})^2 \quad (3)$$

$$E_{y,i} = \sum_{i=1}^N (B_{y \text{ measured},i} - B_{y \text{ model},i})^2 \quad (4)$$

$$E_{z,i} = \sum_{i=1}^N (B_{z \text{ measured},i} - B_{z \text{ model},i})^2 \quad (5)$$

The total objective error is simply the summation across the x, y, z components and individual sensors:

$$E = \sum_{i=1}^N E_{x,i} + E_{y,i} + E_{z,i} \quad (6)$$

By minimizing E through iterative nonlinear least-squares optimization as outlined in [4], [6], the position a, b, c and orientation u, v, w of the magnetic source can be estimated from the array of n sensor measurements.

To evaluate the magnetic field-based tracking scheme, the root mean squared error (RMSE) is used. For a collection of N sample points over a specified trajectory, the positional RMSE is defined as

$$\text{RMSE} = \sqrt{\frac{1}{N} \sum_{j=1}^N \left\{ \begin{array}{l} (a_{\text{estimated},j} - a_{\text{true},j})^2 + \dots \\ \dots + (b_{\text{estimated},j} - b_{\text{true},j})^2 + \dots \\ \dots + (c_{\text{estimated},j} - c_{\text{true},j})^2 \end{array} \right\}} \quad (7)$$

where j ($1 \leq j \leq N$) is an integer representing the sample index, $a_{\text{estimated},j}$ is the estimated position obtained through the nonlinear optimization and $a_{\text{true},j}$ is the actual position.

The MATLAB optimization toolbox (Mathworks, Natick, MA) is used to implement the non-linear optimization algorithm. Unlike the *fmincon* function or *lsqnonlin* with a trust-region-reflective algorithm, *lsqnonlin* with Levenberg-Marquardt algorithm does not require any boundaries to be specified. It is also faster and provides higher accuracy [17]. This is the solver that has been selected. However, because it requires an initial guess of the searched parameters, a *MultiStart* function has been incorporated into the algorithm to avoid a failure in convergence. It generates start points and repeatedly runs the local solver to obtain global minimum and the lowest objective function value.

C. Optimal Sensor Arrangement

A key component that is often overlooked in development of magnetic tracking and localization systems is the spatial placement of the magnetic sensors. In particular, the magnetic field model in (1) specifies that the sensor location be known but does not where it should be. For the procedure of catheter insertion during ventriculostomy, this pertains to the positional distribution of the magnetic sensors on the surface of the skull to detect the catheter tip as it descends into the ventricles. The design method utilized here seeks to determine an optimal set of sensors, and their positions, for a specified path/trajectory. Optimality in localization applications is defined as the spatial arrangement that result in the lowest RMSE in (7).

Without loss of generality, a 2D Cartesian space is defined and constrained to a bounded domain in which the sensors can reside in. This space can be linearly transformed into

curvilinear coordinates for applications with curve surfaces. Another constraint is the physical size of the sensors, which must be considered to prevent their physical footprint from overlapping. For n sensors, the number of combinations to search through can be quite immense. For the ventriculostomy catheter insertion, where the 2D sensor space is delimited to 120×100 mm (limited by the size of the skull) and populated by sensors with a footprint of 5×5 mm, the total number of possible combinations is

$$C_{12221}^n = \frac{12221!}{n!(12221 - n)!} \quad (8)$$

For an arrangement of nine sensors, there are 1.67×10^{31} valid combinations. The sheer number of combinations impedes exploration of all possible combinations using traditional optimization techniques. Hence, two approaches were adopted to tackle the large search domain.

1) *Rectangular Array*: This approach reduces the complexity of the spatial sensor placement by constraining them into the vertices of a rectangular grid within the bounded 2D sensor space as shown in Fig.3(a). While this constraints the number of sensors distributed in the x and y direction, the spacing between sensors in the x and y direction as well as the location of the center of the grid are left unconstrained. For certain n values, multiple configurations may be possible ($n = 10$ permits 2×5 and 5×2 configurations). Using the RMSE as the objective function, contemporary nonlinear optimizing schemes can be used to iteratively determine the unconstrained variables. The main advantage of using a grid to constraint the sensor arrangement is that the number of unconstrained variables is significantly reduced while still maintaining uniform sensor distribution across the 2D sensor domain. Such an approach may be more suitable when the localization path is unknown or irregular but may not be optimal for a specific application such as repetitive catheter insertion trajectories. Moreover, having a rectangular grid pattern restricts the number of sensors in the array. An array of 13 sensors cannot be constrained into a regular grid assembly.

2) *Genetic Algorithm (GA)*: An alternative approach seeks to tackle the large search in space by using GA, which do not place any geometrical constraints on the sensor arrangement and harness the search heuristic of biological

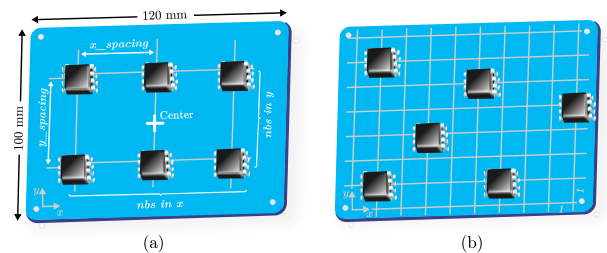


Fig. 3. Sensor arrangement in bounded 2D space. a) Rectangular array: The parameters $xspacing$ and $yspacing$ are the spatial spacing between two sensors and $nbs \text{ in } x$ and $nbs \text{ in } y$ are the number of sensors in x and y direction respectively. b) GA pattern: The positional coordinate of each sensor is (x_i, y_i)

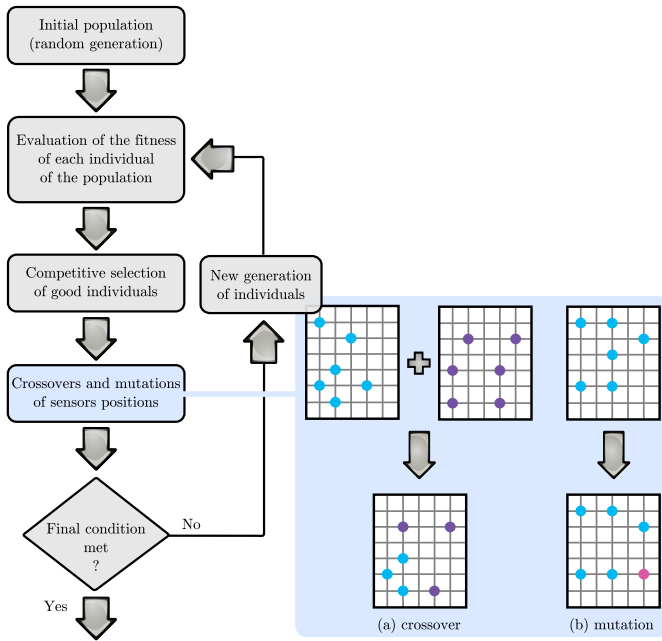


Fig. 4. Flow chart of a GA optimization and genetic operators used to vary the programming of individuals from one generation to the next. (a) Crossover (b) Mutation

natural selection to determine the optimal arrangement of sensors. In GA, an individual is referred to as a genome and the vector entries of an individual as genes. Likewise, a population represents an array of genes. The overall idea behind GAs is to build better genes by somehow combining the "good" parts of other solutions through evolution, just like nature does by recombining the DNA of living beings [10]. Just like other optimization techniques, it uses a fitness/objective function to evaluate the performance of each gene. A flow chart that visually illustrates the principle of GA optimization is presented in Fig. 4. A GA starts with an initial population of genes, which are usually randomized, and calculates the fitness functions of each gene. Using this metric, certain individuals in the current population, called parents, are used to create individuals in the next generation, called children, using crossover and mutation. Crossover is the process where two genes in a population exchange some of their genomes to create a new, third gene. Random substitution of the genome within a gene is defined as mutation.

Adapting GAs into the spatial design of the 2D sensor space requires that the space be first subdivided into a fine grid pattern in which the vertices form nodes. Each node of the grid, which is associated with a coordinate, represents a possible sensor location (x_i, y_i) . Considering each of these coordinates as a genome, a gene is defined as a concatenated vector $(x_1, y_1, \dots, x_i, y_i, \dots, x_n, y_n)$ containing positional coordinates of all sensors. A GA seeks to evolve the gene over generations to produce offspring that minimize the objective/fitness function, which is the RMSE of the positional estimates in (7). A typical spatial sensor arrangement corresponding to an arbitrary gene is shown in

Fig. 3(b). An initial population comprising of a collection of randomized genes were implemented to ensure the diversity of the population for effective crossover and mutation.

III. NUMERICAL SIMULATION

The two approaches in optimal spatial design of the sensor arrangement are numerically evaluated and investigated. The representative trajectory of the inserted ventriculostomy catheter in Fig. 1 comprising of $N = 56$ sample points was used to compute the fitness function in (7). To incorporate robustness to the system, in addition to the N points of the representative path, a buffer zone composed of the spatial points within 10 mm of the trajectory is included for optimization. The magnet is modeled after an axially magnetized NdFeB grade N52 solid cylinder permanent magnet (K&J Magnetics, Jamison, PA) with 3.2 mm diameter and 9.5 mm length (D26-N52). The dipole moment of the magnet m_{DM} was experimentally determined to be $8.66 \times 10^4 \text{ Am}^2$ using field mapping and least-squares analysis detailed in [1]. Both approaches are limited to the 2D sensor space of 120×100 mm and simulate 3-axis magnetic field sensors.

For simulation of the spatial design based on the rectangular grid, the spacing between sensors in the x and y direction varied from 5 to 40 mm (in 1 mm integer increments) and the number of sensors in each direction was an integer between 2 and 10. The center of the grid pattern was permitted to deviate 10 mm (in 1 mm integer increments) from the centroid of the sensor space. In the GA-based design, the node spacing was set to 1 mm and the initial population comprised twice the number of genomes (each genome is an x or y coordinate of a single sensor). A minimum Euclidean spacing between sensors was set to 5 mm to prevent physical interference. This starting population contained randomized genes as well as those derived from the rectangular grid optimization results. In both approaches MATLAB's *lsqnonlin* optimization function was used with the Levenberg-Marquardt algorithm as the solver. The GA-based approach additionally used the *ga* function with the mixed integer optimization programming option to ensure that all components of the gene are integers.

A. Localization Performance Comparison

Table I shows the simulated positional RMSE on the localization of the catheter trajectory using rectangular arrays and GA optimized arrangements for $n = 9$ to 18. The results in Table I are grouped according to the number of sensors implemented. Within each number of sensors, classification was subdivided into different possible configurations for the rectangular arrays. The spatial sensor spacing of each optimally derived configuration is also appended in the table. To visualize best-performing sensor designs, the spatial position of each individual sensor in the 2D sensor space is illustrated in the schematic in Fig. 5 for four selected n values. The schematic also shows (in red) the projected catheter trajectory in the z -plane.

From the Table I, it can be seen that in the absence of noise, the theoretical RMSE of the GA-derived sensor

TABLE I

COMPARISON OF RMSE ACROSS DIFFERENT NO. OF SENSORS AND SENSOR ARRANGEMENT. (* SIMULATION WITH $0.25 \mu\text{T}$ RMS NOISE)

Nb. of sensors	nbX×nbY	Gride size X×Y (mm)	RMSE ($\times 10^{-7}$ mm)		RMSE ($\times 10^{-2}$ mm)	
			Rect.	GA	Rect.*	GA*
9	3 × 3	36 × 20	4.08	1.60	10.96	3.37
10	2 × 5	36 × 26	4.89	2.40	10.85	4.02
	5 × 2	21 × 22	3.88	-	13.02	-
11	-	-	-	-	-	5.23
12	2 × 6	36 × 19	4.65	-	10.67	-
	6 × 2	14 × 27	3.55	2.57	15.52	4.11
	3 × 4	34 × 25	3.87	-	11.81	-
	4 × 3	28 × 16	3.83	-	8.17	-
13	-	-	-	-	-	3.77
14	2 × 7	34 × 14	5.00	2.77	12.21	3.00
	7 × 2	12 × 32	4.46	-	14.49	-
15	3 × 5	31 × 11	3.82	2.84	13.07	3.06
	5 × 3	20 × 24	3.79	-	10.46	-
16	2 × 8	35 × 12	4.98	-	12.85	-
	8 × 2	10 × 35	4.59	2.48	13.32	2.38
	4 × 4	29 × 13	3.70	-	6.93	-
17	-	-	-	-	-	2.29
18	2 × 9	36 × 11	5.04	-	11.86	-
	9 × 2	8 × 33	4.87	2.31	10.99	3.06
	3 × 6	36 × 16	4.05	-	11.60	-
	6 × 3	15 × 20	3.85	-	9.64	-

arrangements are on average 40 % lower than the rectangular grid optimized designs across all sensors. The GA boards were able to average an RMSE of 2.4×10^{-7} mm while the rectangular grid-based boards could only muster an average of 4.2×10^{-7} mm. Moreover, there is no visible correlation between the number of sensors and RMSE. The best performing rectangular grid board was a 3×4 configuration of 12 sensors, while the best GA-based board had nine sensors board. This difference was anticipated because the numerical effects of sensors are only visible in presence of noise.

A second simulation was performed while the measurement signals of the sensors were corrupted by a Gaussian noise with a standard deviation of $\pm 0.25 \mu\text{T}$, corresponding to the noise characteristics of a commercial magnetometer: MAG3110 (Freescale Semiconductor, Austin, TX). The RMSE resulting from this simulation are also appended in Table I. To facilitate comparison, Fig. 6 shows the variation of RMSE across the number of sensors in the presence of noise. As expected, the RMSE decreased as the number of sensors increased for both design approaches. However, when depicted by the graph, the advantage of the GA-based board over a rectangular grid-based board are more noticeable. To put the data in perspective, a six-sensor GA optimized board has a comparable RMSE to a 20-sensor rectangular grid-optimized board (0.065 mm vs 0.058 mm). As shown in Fig. 7, rather than increasing the number of sensors on the rectangular grid designs, it is more advantageous to pursue a GA-based design.

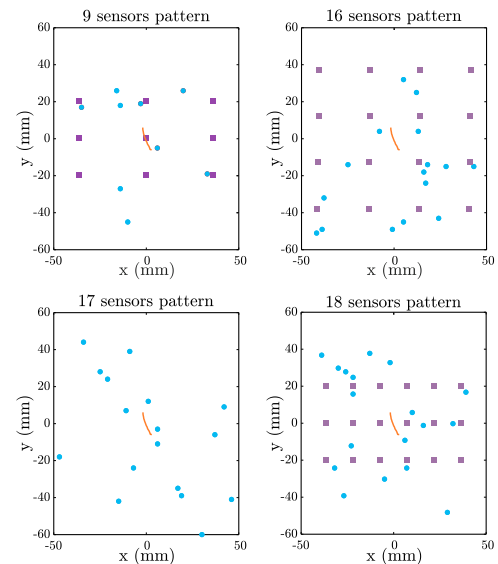


Fig. 5. Comparison of Rectangular and GA-derived sensor arrangements. Blue dots and purple squares represent individual sensor positions in the GA-based and rectangular grid designs.

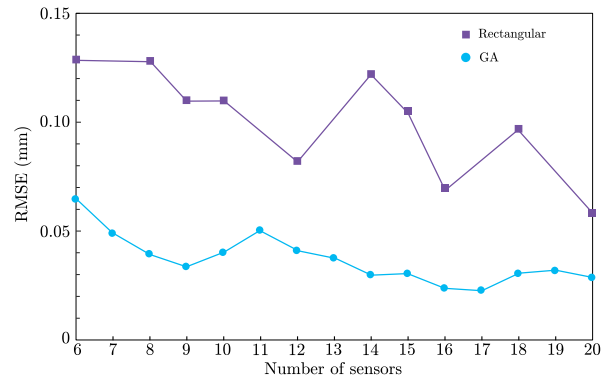


Fig. 6. Localization RMSE as a function of number sensors in presence of Gaussian measurement noise.

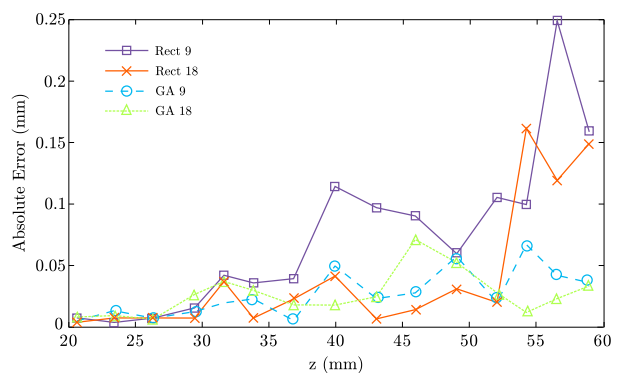


Fig. 7. Absolute positional estimation error at various z displacement across the trajectory path with four different simulated patterns.

IV. EXPERIMENTAL INVESTIGATION

To experimentally verify the simulation results, 6-axis articulated robotic arm (VS-068, Denso Robotics, Aichi, Japan) was used with a D26-N52 permanent magnet (same

as in the simulations) mounted at the end-effector of the articulated arm (Fig. 8). Each of the six servomotors and encoders on the robotic arm were powered and controlled using an integrated amplifier/controller (RC7, Denso Robotics, Aichi, Japan). The robotic arm has a positional repeatability of 0.02 mm. Customized sensor boards, containing an arrangement of 3-axis magnetic sensors (MAG3110, Freescale Semiconductor, Austin, TX) and accompanying electronics were affixed to the base. These digital sensors have a resolution of $0.10 \mu\text{T}$ within a range of $\pm 1000 \mu\text{T}$ and powered by a highly accurate, low-noise DC power supply at 3.3V (GS200, Yokogawa, Tokyo, Japan). The electrical schematic for the magnetic sensor on the sensor board is shown in Fig. 9. Three boards (9 and 18-sensor rectangular grid boards and a 9-sensor GA board) were built according to the designs obtained in the simulation experiments as shown in Fig. 10.

A high performance field programmable grid array (FPGA) with a real-time controller (cRIO 9082, National Instruments (NI), Austin, USA) was interfaced between the sensor boards and the robot controller. The magnetic field measurements were transmitted through I2C protocol and acquired using a digital I/O module (NI9403, NI, Austin, TX) installed on the real-time controller. Motion commands to the robot controller were transmitted via an Ethernet connection. Programming of the FPGA-powered controller and the attached module was achieved with LabVIEW (NI, Austin, TX) and the ImagingLab Robotics Library (ImagingLab GmbH, Alzenau, Germany) provided the software protocol to communicate with the robot arm controller directly from LabVIEW.

A. Localization Performance Verification

The end-effector of the articulated arm was programmed using the robot controller to follow a trajectory that is similar to but not identical to the representative path of the sensor board. Along the trajectory, the field measurements acquired by the sensors were recorded and used to estimate the position of the magnet and subsequently compared to the actual position of the end-effector of the robotic arm. A total of 15 data points were collected during the trajectory and the absolute error of the positional estimates at each sample point as a function of the z coordinate of the sample point are shown in Fig. 11 demonstrating that the trajectory goes to a Euclidean depth of 60 mm, well over that required for ventriculostomy. The RMSE of the three boards are consolidated in Table II.

The RMSE and spatial absolute error plots in Table II and Fig. 11 fully support the trend observed in the simulations. The localization performance of 9-sensor GA derived board was comparable to the 18-sensor rectangular grid board and appreciably outperformed the 9-sensor rectangular grid board. Although the magnitude of the errors were higher than those predicted by the simulations, the errors can be attributed to the imperfect magnetic source, field modeling errors, sensor non-linearity and background noise. These were especially acute for locations that are further away,

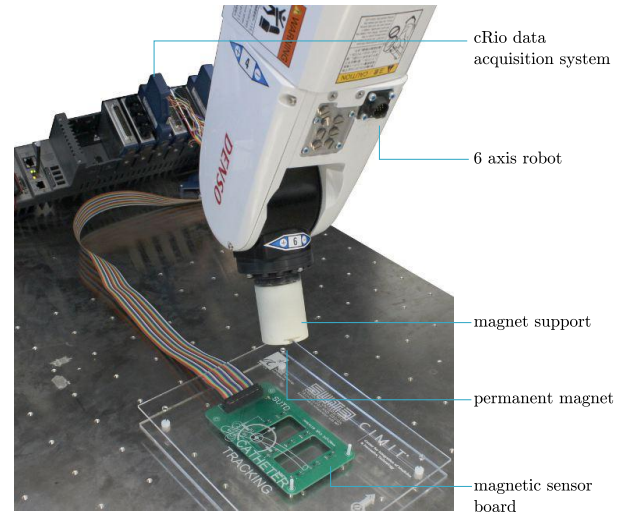


Fig. 8. Experimental setup consisting of a 6-axis robot arm with N52 cylindrical magnet at the end-effector and a magnetic sensor board affixed onto the worktable.

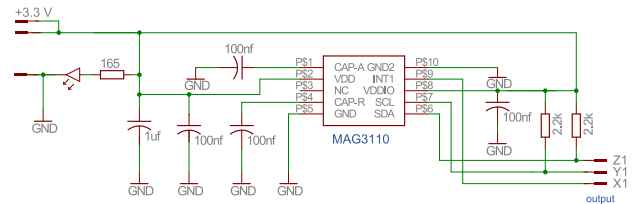


Fig. 9. MAG3110 electrical schematics.

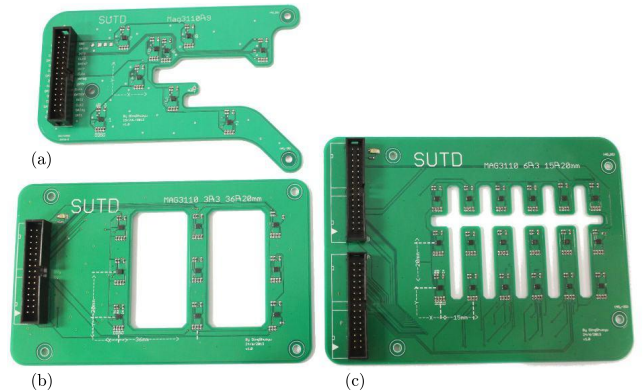


Fig. 10. Experimental sensor boards. (a) Nine-sensor GA (b) Nine-sensor rectangular (c) Eighteen-sensor rectangular

due to the reduced SNR. With proper sensor calibration and improved field modeling, these errors can be reduced.

V. CONCLUSION

A scheme to determine the optimal spatial sensor configuration of a permanent magnet localization system for enhanced tracking performance is presented. This approach uses Genetic Algorithms and encodes the sensor layout

TABLE II
EXPERIMENTAL LOCALIZATION COMPARISON

Number of Sensors	RMSE (mm)	
	Rectangular pattern	GA pattern
9	4.69	4.12
18	4.10	–

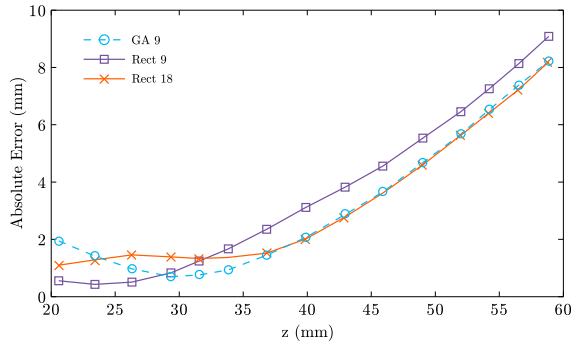


Fig. 11. Experimental error comparison at various z displacements along the trajectory points.

as a gene so that an optimal sensor configuration can be iteratively calculated through evolution of the gene pool. The simulated and experimental performance of a sensing system using a GA-derived configuration is superior to an optimized grid layout often used in current systems. The results also suggest that sensor layout design has a larger influence on localization accuracy and is more efficient than the traditional option of installing and employing additional sensors. In this paper, optimal design has been investigated with planar arrays of sensors for simplicity of validation. Nevertheless, the method is extendable to accommodate systems with more complex geometries and also in 3 dimensions. Next steps include implementing the optimized sensor layout on a 3D flexible support that is compliant which allows it to be fitted directly onto the convex surfaces of the head.

ACKNOWLEDGMENT

The authors are grateful to the Agency for Science, Technology and Research (A*STAR) and the Center for Integration of Medicine & Innovative Technology (CIMIT) for supporting this research work. In addition, we would like to thank the Mass General/North Shore Center for Outpatient Care, Danvers, MA.

REFERENCES

[1] F. Wu, N. M. Robert, and S. Foong, "Enhanced Magnetic Localization with Artificial Neural Network Field Models." in *IEEE International*

Conference on Robotics and Automation (ICRA), Karlsruhe, Germany, 2013.

[2] F. Wu, D. D. Frey, and S. Foong, "A hybrid magnetic field model for axisymmetric magnets," in *Advanced Intelligent Mechatronics (AIM), 2013 IEEE/ASME International Conference on*, 2013, pp. 786–791.

[3] D. Roberts, "Is good good enough?" *Neurocritical care*, vol. 10, pp. 155–156, 2009.

[4] C. Hu, M.-H. Meng, M. Mandal, and X. Wang, "3-Axis Magnetic Sensor Array System for Tracking Magnet's Position and Orientation." in *Intelligent Control and Automation, 2006. WCICA 2006. The Sixth World Congress on*, vol. 2, 2006, pp. 5304–5308.

[5] C. Hu, W. Yang, D. Chen, M. Q. H. Meng, and H. Dai, "An improved magnetic localization and orientation algorithm for wireless capsule endoscope." in *Conference proceedings : ... Annual International Conference of the IEEE Engineering in Medicine and Biology Society. IEEE Engineering in Medicine and Biology Society. Conference*, vol. 2008, no. 1, Jan. 2008, pp. 2055–8.

[6] V. Schlageter, P.-A. Besse, R. S. Popovic, and P. Kucera, "Tracking system with five degrees of freedom using a 2D-array of Hall sensors and a permanent magnet." *Sensors and Actuators A: Physical*, vol. 92, no. 13, pp. 37–42, 2001.

[7] V. Schlageter, P. Drljaca, R. S. Popovic, and P. Kucera, "A Magnetic Tracking System based on Highly Sensitive Integrated Hall sensors." *JSME International Journal Series C*, vol. 45, no. 4, pp. 967–973, 2002.

[8] C. Hu, M. Q. Meng, and M. Mandal, "Efficient magnetic localization and orientation technique for capsule endoscopy." in *Intelligent Robots and Systems, 2005. (IROS 2005). 2005 IEEE/RSJ International Conference on*, 2005, pp. 628–633.

[9] S. Foong, K.-M. Lee, and K. Bai, "Harnessing Embedded Magnetic Fields for Angular Sensing With Nanodegree Accuracy," *Mechatronics, IEEE/ASME Transactions on*, vol. 17, no. 4, pp. 687–696, 2012.

[10] D. E. Goldberg, *Genetic Algorithms in Search, Optimization, and Machine Learning*. Pearson Education, 1989.

[11] A. Ehtisham, S. Taylor, L. Bayless, M. W. Klein, and J. M. Janzen, "Placement of external ventricular drains and intracranial pressure monitors by neurointensivists." *Neurocritical care*, vol. 10, no. 2, pp. 241–247, 2009.

[12] P. P. Banerjee, C. J. Luciano, G. M. Lemole, F. T. Charbel, and M. Y. Oh, "Accuracy of ventriculostomy catheter placement using a head- and hand-tracked high-resolution virtual reality simulator with haptic feedback." *Journal of neurosurgery*, vol. 107, no. 3, pp. 515–21, Sept. 2007.

[13] C. A. Schneider, W. S. Rasband, and K. W. Eliceiri, "NIH Image to ImageJ: 25 years of image analysis," *Nature Methods*, vol. 9, no. 7, pp. 671–675, 2012.

[14] P. A. Yushkevich, J. Piven, H. Cody Hazlett, R. Gimpel Smith, S. Ho, J. C. Gee, and G. Gerig, "User-Guided 3D Active Contour Segmentation of Anatomical Structures: Significantly Improved Efficiency and Reliability," *Neuroimage*, vol. 31, no. 3, pp. 1116–1128, 2006.

[15] W. Weitschies, J. Wedemeyer, R. Stehr, and L. Trahms, "Magnetic markers as a noninvasive tool to monitor gastrointestinal transit," *Biomedical Engineering, IEEE Transactions on*, vol. 41, no. 2, pp. 192–195, 1994.

[16] M. Li, S. Song, C. Hu, D. Chen, and M.-H. Meng, "A novel method of 6-DoF electromagnetic navigation system for surgical robot," in *Intelligent Control and Automation (WCICA), 2010 8th World Congress on*, Jinan, China, 2010, pp. 2163–2167.

[17] S. Song, C. Hu, M. Li, W. Yang, and M. Q.-H. Meng, "Real time algorithm for magnet's localization in capsule endoscope," in *IEEE International Conference on Automation and Logistics*, Shenyang, China, 2009, pp. 2030–2035.